Coherent optical OFDM: theory and design

W. Shieh, H. Bao, and Y. Tang

ARC Special Research Centre for Ultra-Broadband Information Networks and National ICT Australia
Department of Electrical and Electronic Engineering
The University of Melbourne, Melbourne, VIC 3010, Australia
e-mail: w.shieh@ee.unimelb.edu.au

Abstract: Coherent optical OFDM (CO-OFDM) has recently been proposed and the proof-of-concept transmission experiments have shown its extreme robustness against chromatic dispersion and polarization mode dispersion. In this paper, we first review the theoretical fundamentals for CO-OFDM and its channel model in a 2x2 MIMO-OFDM representation. We then present various design choices for CO-OFDM systems and perform the nonlinearity analysis for RF-to-optical up-converter. We also show the receiver-based digital signal processing to mitigate self-phase-modulation (SPM) and Gordon-Mollenauer phase noise, which is equivalent to the mid-span phase conjugation.

OCIS codes: (060.1660) Coherent communications; (0606.5060) Phase modulation

References and links

1. W. Shieh and C. Athaudage, "Coherent optical orthogonal frequency division multiplexing," Electron. Lett. **42**, 587-589 (2006).
2. S. Hara and R. Prasad, *Multicarrier Techniques for 4G Mobile Communications* (Artech House, Boston, 2003).
3. W. Shieh, "PMD-supported coherent optical OFDM systems," IEEE Photon.Technol. Lett. **19**, 134-136 (2007).
4. W. Shieh, X. Yi, and Y. Tang, "Transmission experiment of multi-gigabit coherent optical OFDM systems over 1000 km SSMF fiber," Electron. Lett. **43**, 183-185 (2007).
5. S. L. Jansen, I. Morita, N. Takeda, and H. Tanaka; "20-Gb/s OFDM transmission over 4,160-km SSMF enabled by RF-Pilot tone phase noise compensation," in Optical Fiber Communication Conference and Exposition and The National Fiber Optic Engineers Conference, Technical Digest, (Anaheim, CA, USA, 2007), Paper PDP15.
6. W. Shieh, X. Yi, Y. Ma, and Y. Tang, "Theoretical and experimental study on PMD-supported transmission using polarization diversity in coherent optical OFDM systems," Opt. Express **15**, 9936-9947 (2007).
7. A. J. Lowery and J. Armstrong, "10 Gb/s multimode fiber link using power-efficient orthogonal-frequency-division multiplexing," Opt. Express **13**, 10003–10009 (2005).
8. J. M. Tang, P. M. Lane, and K. A. Shore, "Transmission performance of adaptively modulated optical OFDM signals in multimode fiber links," IEEE Photon. Technol. Lett. **18**, 205–207 (2006).
9. J. M. Tang, J.M., P.M. Lane, K. A. Shore, "30 Gb/s transmission over 40 km directly modulated DFB laser-based SMF links without optical amplification and dispersion compensation for VSR and metro applications," Optical Fiber Commun. Conf., Anaheim, CA, paper JThB8 (2006).
10. A. J. Lowery, L. Du, and J. Armstrong, "Orthogonal frequency division multiplexing for adaptive dispersion compensation in long haul WDM systems," Optical Fiber Commun. Conf., Anaheim, CA, paper PDP39 (2006).
11. I. B. Djordjevic and B. Vasic, "Orthogonal frequency division multiplexing for high-speed optical transmission," Opt. Express **14**, 3767–3775 (2006).
12. R. W. Chang, "Synthesis of band-limited orthogonal signals for multichannel data transmission," Bell Sys. Tech. J. **45**, 1775-1796 (1966).
13. B. R. Saltzberg, "Performance of an efficient parallel data transmission system," IEEE Trans. Commun. **15**, 805-813 (1967).
14. S. B. Weinsten and P. M. Ebert, "Data transmission by frequency-division multiplexing using the discrete

#86668 - $15.00 USD Received 20 Aug 2007; revised 1 Nov 2007; accepted 5 Nov 2007; published 9 Jan 2008

frouer transform," IEEE Trans. Commun. **19**, 628-634 (1971).
15. L. Hanzo, M. Munster, B. J. Choi, and T. Keller, *OFDM and MC-CDMA for Broadband Multi-User Communications, WLANS and Broadcasting*, (John Wiley & Sons, West Sussex, 2003).
16. Y. Li, L. J. Cimini, and N. R. Sollenberger, "Robust channel estimation for OFDM systems with rapid dispersive fading channels," IEEE Trans. On Commun. **46**, 902-915 (1998).
17. Y. Tang, W. Shieh, X. Yi and R. Evans, "Optimum design for RF-to-optical up-converter in coherent optical OFDM systems," IEEE Photon. Technol. Lett. **19**, 483 – 485 (2007).
18. D. S. Ly-Gagnon, S. Tsukarnoto, K. Katoh, and K. Kikuchi, "Coherent detection of optical quadrature phase-shift keying signals with carrier phase estimation," J. Lightwave Technol. **24**, 12-21 (2006).
19. S. J. Savory, G. Gavioli, R. I. Killey, and P. Bayvel, "Electronic compensation of chromatic dispersion using a digital coherent receiver," Opt. Express **15**, 2120-2126 (2007).
20. X. Yi, W. Shieh, and Y. Ma, "Phase noise on coherent optical OFDM systems with 16-QAM and 64-QAM beyond 10 Gb/s," European Conference on Optical Communications, paper 5.2.3, Berlin, Germany (2007).
21. B.R. Washburn, S.A. Diddams, N.R. Newbury, J.W. Nicholson, M.F. Yan, and C.G. Jorgensen, "Phase-locked, erbium-fiber-laser-based frequency comb in the near infrared," Optics Lett. **29**, pp. 250-252 (2004).
22. A. Sano, E. Yoshida, H. Masuda, T. Kobayashi, E. Yamada, Y. Miyamoto, F. Inuzuka, Y. Hibino, Y. Takatori, K. Hagimoto, T. Yamada, and Y. Sakamaki, "30 x 100-Gb/s all-optical OFDM transmission over 1300 km SMF with 10 ROADM nodes," European Conference on Optical Communications, paper PD1.7, Berlin, Germany (2007).
23. A. D. Ellis, and F. C. G. Gunning, "Spectral density enhancement using coherent WDM," IEEE Photon. Technol. Lett. **17**, 504-506 (2005).
24. S. Wu and Y. Bar-Ness, "A phase noise suppression algorithm for OFDM-based WLANs," IEEE Commun. Lett. **6**, pp. 535–537 (2002).
25. N. Gisin, and B. Huttner, "Combined effects of polarization mode dispersion and polarization dependent losses in optical fibers," Optics Commun. **142**, 119-125 (1997).
26. L. Tomba, "The effect of Wiener phase noise in OFDM systems," IEEE Trans. Commun. **46**, 580-583 (1998).
27. W. Shieh, "Maximum-Likelihood Phase Estimation for Coherent Optical OFDM," European conference on optical communication, paper 4.2.5, Berlin, Germany (2007).
28. X. Yi, W. Shieh, and Y. Tang, "Phase Estimation for Coherent Optical OFDM," IEEE Photon. Technol. Lett. **19**, pp. 919 – 921 (2007).
29. Y. Han and G. Li, "Coherent optical communication using polarization multiple-input-multiple-output," Optics Express **13**, 7527-7534 (2005).
30. F. Auracher and R. Keil, "Method for measuring the RF modulation characteristics of Mach-Zehnder-type modulators," Appl. Phys. Lett. **36**, 626-629 (1980).
31. B. H .Kolner and D. W. Dolfi, "Intermodulation distortion and compression in an integrated electrooptic modulator," Appl. Optics **26**, 3676-3680 (1987).
32. M. Mayrock and H. Haunstein, "Impact of Implementation Impairments on the Performance of an Optical OFDM Transmission System," European Conference on Optical Communications, paper Th3.2.1, Cannes, France (2006).
33. H. Bao and W. Shieh, "Transmission simulation of coherent optical OFDM signals in WDM systems," Opt. Express **15**, 4410-4418 (2007).
34. K. Roberts, "Electronic Dispersion Compensation beyond 10 Gb/s" Technical Digest, LEOS Summer Topical Meeting, paper MA2.3 (2007).
35. S. Watanabe and M. Shirasaki, "Exact compensation for both chromatic dispersion and kerr effect in a transmission fiber using optical phase conjugation," J. Lightwave Technol. **14**, 243–248 (1996).
36. S. L. Jansen, D. van den Borne, C. C. Monsalve, S. Spalter, P.M. Krummrich, G. D. Khoe, and H. de Waardt, "Reduction of Gordon-Mollenauer phase noise by midlink spectral inversion," IEEE Photon. Technol. Lett. **17**, 923–925 (2005).
37. G. P. Agrawal, *Nonlinear Fiber Optics* (Acadmic Press, San Diego, 1995).
38. G. Charlet, N. Maaref, J. Renaudier, H. Mardoyan, P. Tran, and S. Bigo, "Transmission of 40Gb/s QPSK with coherent detection over ultra long haul distance improved by nonlinearity mitigation," European Conference on Optical Communications, paper Th.4.3.6, Cannes, France (2006).

1. Introduction

There are two trends which are ever evident in today's optical networks: (i) the transmission data rate per channel has been fast increasing and rapidly approaching 100 Gb/s, and (ii) the dynamically reconfigurable network has gradually become a reality thanks to deployment of optical Add/Drop Multiplexers (OADM). These trends place significant challenges to the high-speed transmission link for the optical networks. In particular, as the transmission rate approaches 100 Gb/s, conventional meticulous per-span optical dispersion compensation becomes too costly and time-consuming if not possible, as the dispersion compensation

#86668 - $15.00 USD Received 20 Aug 2007; revised 1 Nov 2007; accepted 5 Nov 2007; published 9 Jan 2008

requires precise fiber dispersion measurement and precise matching of the dispersion compensation cross broad wavelength range. Most importantly, a dynamically reconfigurable network mandates a fast link setup and leaves the manual optical dispersion compensation impractical. Coherent optical orthogonal frequency-division multiplexing (CO-OFDM) has been recently proposed in response to the above-mentioned challenges [1]. OFDM is a multi-carrier transmission technique where a data stream is carried with many lower-rate subcarrier tones [2]. It has emerged as the leading physical-layer interface in wireless communications in the last decade. OFDM has been widely studied in mobile communications to combat hostile frequency-selective fading and has been incorporated into wireless network standards (802.11a/g WiFi, HiperLAN2, 802.16 WiMAX) and digital audio and video broadcasting (DAB and DVB-T) in Europe, Asia, Australia, and other parts of the world. CO-OFDM combines the advantages of 'coherent detection' and 'OFDM modulation' and posses many merits that are critical for future high-speed fiber transmission systems. First, the chromatic dispersion and polarization mode dispersion (PMD) of the transmission system can be effectively estimated and mitigated. Second, the spectra of OFDM subcarriers are partially overlapped, resulting in high optical spectral efficiency. Third, by using direct up/down conversion, the electrical bandwidth requirement can be greatly reduced for the CO-OFDM transceiver, which is extremely attractive for the high-speed circuit design, where electrical signal bandwidth dictates the cost. At last, the signal processing in the OFDM transceiver can take advantage of the efficient algorithm of Fast Fourier Transform (FFT)/Inverse Fast Fourier Transform (IFFT), which suggests that OFDM has superior scalability over the channel dispersion and data rate. CO-OFDM was first proposed to combat chromatic dispersion [1]. It was soon extended to polarization-diversity detection, and has been shown to be resilient to fiber PMD [3]. The first CO-OFDM transmission experiment has been reported for 1000 km SSMF transmission at 8 Gb/s [4], and more CO-OFDM transmission experiment has quickly been reported for 4160 km SSMF transmission at 20 Gb/s [5]. The first CO-OFDM transmission with polarization-diversity has recently been demonstrated showing record PMD tolerance [6]. In the same report [6], the first experiment of nonlinearity mitigation has also been reported for CO-OFDM systems. Although this paper places a focus on the coherent flavour of optical OFDM, we would like to stress that the direct detection flavour of optical OFDM has also been actively pursued by other groups, with applications including multimode fiber transmission [7-8], short-haul single-mode transmission [9], and long haul transmission [10-11].

In this paper, we focus our attention on the theory and design aspects of CO-OFDM. We first review the theoretical fundamentals for CO-OFDM. We then present various design choices for CO-OFDM systems as well as the nonlinearity analysis for the OFDM RF-to-optical up-converter. We also show the receiver-based digital signal processing to mitigate self-phase modulation (SPM) and Gordon-Mollenauer phase noise.

2. **Theoretical fundamentals for CO-OFDM**

2.1 Principle of orthogonal frequency-division multiplexing (OFDM)

OFDM is a special form of a broader class of multi-carrier modulation (MCM), a generic implementation of which is depicted in Fig. 1. The structure of a complex mixer (IQ modulator/demodulator), which is commonly used in MCM systems, is also shown in the figure. The MCM transmitted signal $s(t)$ is represented as

$$s(t) = \sum_{i=-\infty}^{+\infty} \sum_{k=1}^{N_{sc}} c_{ki} s_k \left(t - iT_s\right) \tag{1}$$

#86668 - $15.00 USD Received 20 Aug 2007; revised 1 Nov 2007; accepted 5 Nov 2007; published 9 Jan 2008

$$s_k(t) = \Pi(t)\exp(j2\pi f_k t) \tag{2}$$

$$\Pi(t) = \begin{cases} 1, & (0 < t \le T_s) \\ 0, & (t \le 0,\ t > T_s) \end{cases} \tag{3}$$

where c_{ki} is the ith information symbol at the kth subcarrier, s_k is the waveform for the kth subcarrier, Nsc is the number of subcarriers, f_k is the frequency of the subcarrier, and T_s is the symbol period. The optimum detector for each subcarrier could use a filter that matches the subcarrier waveform, or a correlator matched to the subcarrier as shown in Fig. 1. Therefore, the detected information symbol c'_{ik} at the output of the correlator is given by

$$c'_{ki} = \int_0^{T_s} r(t - iT_s)s^*_k dt = \int_0^{T_s} r(t - iT_s)\exp(-j2\pi f_k t)dt \tag{4}$$

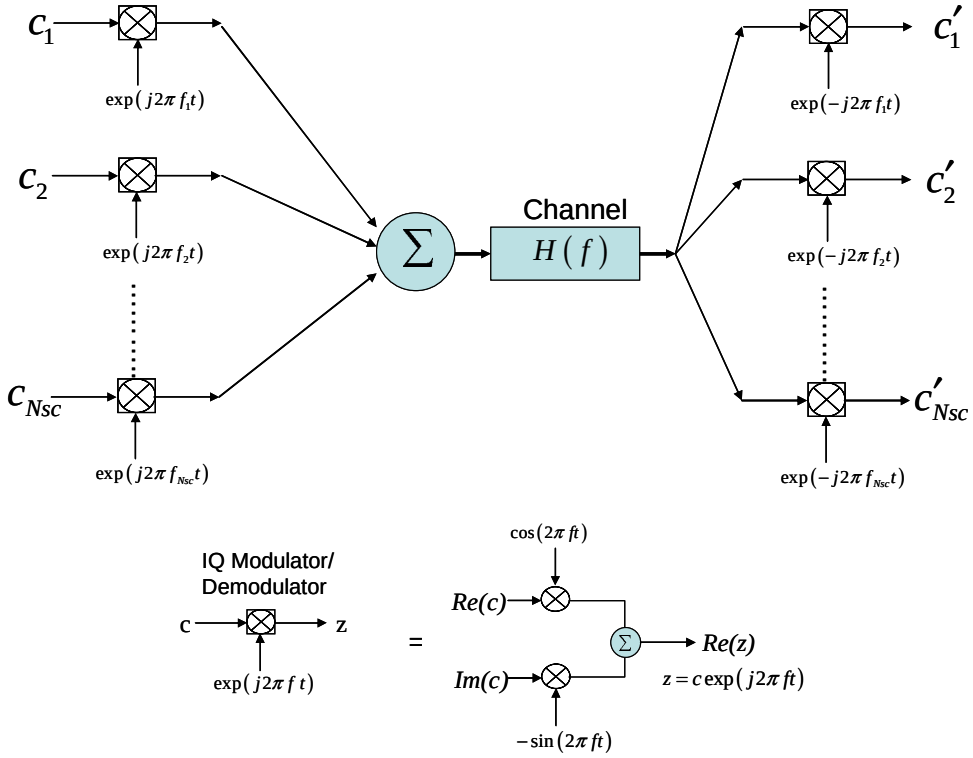

Fig. 1. Conceptual diagram for a generic multi-carrier modulation (MCM) system

where $r(t)$ is the received time-domain signal. The classical MCM uses non-overlapped band-limited signals, and can be implemented with a bank of large number of oscillators and filters at both transmit and receive end. The major disadvantage of MCM is that it requires excessive bandwidth. This is because in order to design the filters and oscillators cost-efficiently, the channel spacing has to be multiple of the symbol rate, greatly reducing the spectral efficiency. A novel approach called orthogonal frequency-division multiplexing (OFDM) was

#86668 - $15.00 USD Received 20 Aug 2007; revised 1 Nov 2007; accepted 5 Nov 2007; published 9 Jan 2008

investigated employing overlapped yet orthogonal signal set [12-13]. This orthogonality originates from the straightforward correlation between any two subcarriers, given by

$$\delta_{kl} = \frac{1}{T_s}\int_0^{T_s} s_k s^*_l dt = \frac{1}{T_s}\int_0^{T_s} \exp\left(j2\pi\left(f_k - f_l \right)t\right)dt$$
$$= \exp\left(j\pi\left(f_k - f_l \right)T_s\right)\frac{\sin\left(\pi\left(f_k - f_l \right)T_s\right)}{\pi\left(f_k - f_l \right)T_s} \tag{5}$$

It can be seen that if the following condition

$$f_k - f_l = m\frac{1}{T_s} \tag{6}$$

is satisfied, then the two subcarriers are orthogonal to each other. This signifies that these orthogonal subcarrier sets, with their frequencies spaced at multiple of inverse of the symbol rate can be recovered with the matched filters (Eq. 4) without inter-carrier interference (ICI), in spite of strong signal spectral overlapping.

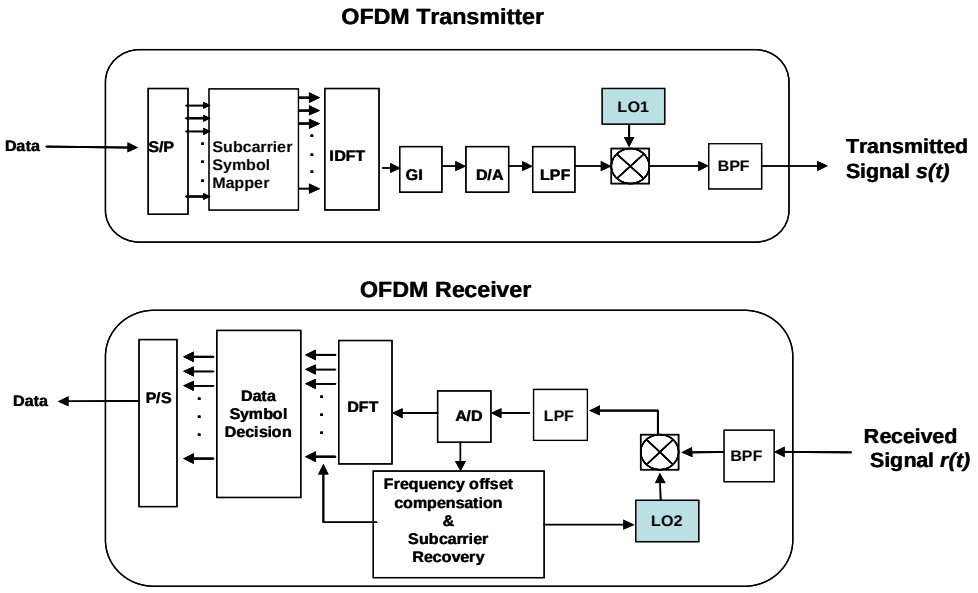

Fig. 2. Conceptual diagram for the OFDM transmitter and receiver

A fundamental challenge with the OFDM is that a large number of subcarriers are needed so that the transmission channel affects each subcarrier as a flat channel. This leads to an extremely complex architecture involving many oscillators and filters at both transmit and receive end. Weinsten and Ebert first revealed that OFDM modulation/demodulation can be implemented by using Inverse Discrete Fourier Transform (IDFT)/Discrete Fourier Transform (DFT) [14]. This is evident by studying OFDM modulation (Eq. 1) and OFDM demodulation (Eq. 4). It follows that the modulation can be performed by IDFT of the input information

#86668 - $15.00 USD Received 20 Aug 2007; revised 1 Nov 2007; accepted 5 Nov 2007; published 9 Jan 2008

symbol c_{ki}, and the demodulation by DFT of the sampled received signal $r(t)$. The corresponding architecture using DFT/IDFT and digital-to-analog/analog-to-digital converter (DAC/ADC) are shown in Fig. 2. At the transmit end, the input data bits are mapped onto corresponding information symbols of the subcarriers within one OFDM symbol, and the digital time domain signal is obtained by using IDFT, which is subsequently inserted with guard interval and converted into real time waveform through DAC. The guard interval is inserted to prevent inter-symbol-interference (ISI) due to channel dispersion. The baseband signal can be up-converted to an appropriate RF band with an IQ mixer/modulator. At the receive end, the OFDM signal is first down-converted to baseband with an IQ demodulator, and sampled with an ADC, and demodulated by performing DFT and baseband signal processing to recover the data.

2.2 Cyclic prefix for OFDM

One of the enabling techniques for OFDM is the insertion of cyclic prefix [2]. Let us first consider two consecutive OFDM symbols that undergo a dispersive channel with a delay spread of t_d. For simplicity, each OFDM symbol includes only two subcarriers with the fast delay and slow delay differenced at t_d, represented by 'fast subcarrier' and 'slow subcarrier', respectively. Figure 3(a) shows that inside each OFDM symbol, the two subcarriers, 'fast subcarrier' and 'slow subcarrier' are aligned upon the transmission. Figure 3(b) shows the same OFDM signals upon the reception where the 'slow carrier' is delayed by t_d against the 'fast carrier'. We select a DFT window containing a complete OFDM symbol for the 'fast subcarrier'. It is apparent that due to the channel dispersion, the 'slow subcarrier' has crossed the symbol boundary leading to the interference between neighboring OFDM symbols, formally, the inter-symbol-interference (ISI). Furthermore, because the OFDM waveform in the DFT window for 'slow subcarrier' is incomplete, the critical orthogonality for the subcarriers is lost, resulting in an inter-carrier-interference (ICI) penalty.

Cyclic prefix was proposed to resolve the channel dispersion induced ISI and ICI [2]. Fig. 3(c) shows insertion of a cyclic prefix by cyclic extension of the OFDM waveform into the guard interval, Δ_G . As shown in Fig. 3(c), the waveform in the guard interval is essentially an identical copy of that in the DFT window, with time-shifted by 't_s' behind. Figure 3(d) shows the OFDM signal with the guard interval upon reception. Let us assume that the signal has traversed the same dispersive channel, and the same DFT window is selected containing a complete OFDM symbol for the 'fast subcarrier' waveform. It can be seen from Fig. 3(d), a complete OFDM symbol for 'slow subcarrier' is also maintained in the DFT window, because a proportion of the cyclic prefix has moved into the DFT window to replace the identical part that has shifted out. As such, the OFDM symbol for 'slow subcarrier' is an 'almost' identical copy of the transmitted waveform with an additional phase shift. This phase shift is dealt with through channel estimation and will be subsequently removed for symbol decision. Now we arrive at the important condition for ISI-free OFDM transmission, given by

$$t_d < \Delta_G \tag{7}$$

#86668 - $15.00 USD Received 20 Aug 2007; revised 1 Nov 2007; accepted 5 Nov 2007; published 9 Jan 2008

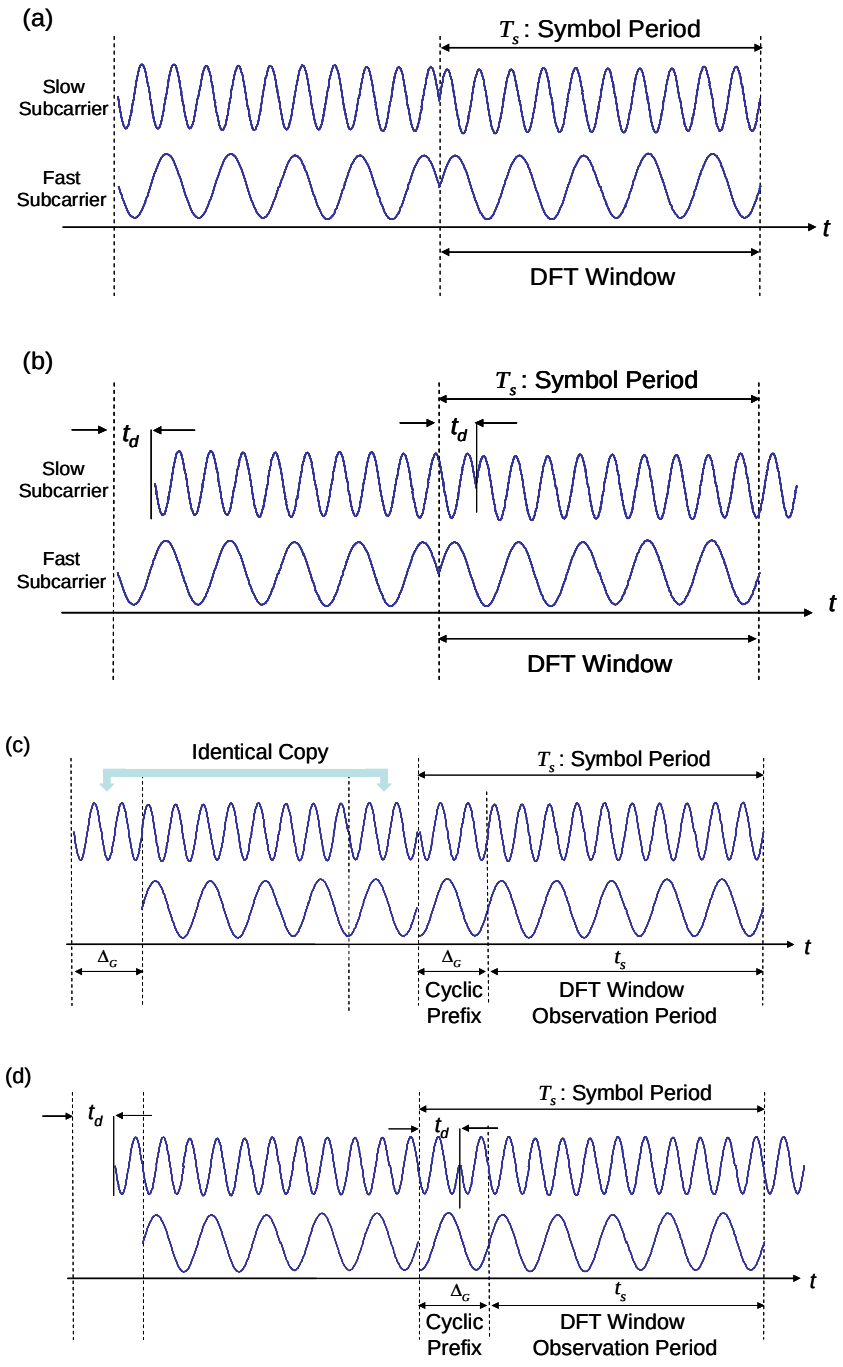

Fig. 3. The OFDM signals (a) without cyclic prefix at the transmitter, (b) without cyclic prefix at the receiver, (c) with cyclic prefix at the transmitter, and (d) with cyclic prefix at the receiver.

It can be seen that to recover the OFDM information symbol properly, there are two critical procedures that need to be carried out, (i) selection of an appropriate DFT window,

#86668 - $15.00 USD Received 20 Aug 2007; revised 1 Nov 2007; accepted 5 Nov 2007; published 9 Jan 2008

called DFT window synchronization, and (ii) estimation of the phase shift for each subcarrier, called channel estimation or subcarrier recovery. Both signal processing procedures are actively-pursued research topics, and the their references can be found in books and journal papers [2, 15,16].

2.3 Principle of coherent optical OFDM

Because of its extreme resilience to the channel dispersion, OFDM has been actively explored for applications in the optical domain. The most critical assumption for OFDM is the linearity in modulation, transmission, and demodulation. Consequently, a linear transformation is the key goal for the OFDM implementation. A generic optical OFDM system can be divided into five functional blocks including (i) the RF OFDM transmitter, (ii) the RF-to-optical (RTO) up-converter, (iii) the optical channel, (iv) the optical-to-RF (OTR) down-converter, and (v) the RF OFDM receiver [1]. The detailed architecture for the RF OFDM transmitter/receiver has been shown in Fig. 2, which generates/recovers the OFDM signals either in baseband or RF band. Let us assume for now a linear optical fiber channel where the fiber nonlinearity is not considered. It is apparent that the challenges for CO-OFDM implementation are to obtain a linear RTO up-converter and linear OTR down-converter. It has been proposed and analyzed that by biasing the Mach-Zehnder modulators (MZMs) at null point, a linear conversion between the RF signal and optical field signal can be achieved [1,17]. We will further treat this important issue of the (non)linearity of the RTO up-converter in section 4. It has also been shown that by using coherent detection, a linear transformation from optical field signal to RF (or electrical) signal can be achieved [1,18,19]. Now by putting together such a composite system cross RF and optical domain [1,17], a linear channel can be constructed where OFDM can perform its best, i.e., mitigating channel dispersion impairment, in both RF domain and optical domain. We will present a channel model for such a composite system cross RF and optical domain in the section 3. In this paper, we use the term 'RF domain' and 'electrical domain' interchangeably.

2.4 Optical spectral efficiency for CO-OFDM

In CO-OFDM systems, *Nsc* subcarriers are transmitted in every OFDM symbol period of T_s. Thus the total symbol rate *R* for CO-OFDM systems is given by

$$R = N_{sc} / T_s \tag{8}$$

Figure 4(a) shows the spectrum of wavelength-division-multiplexed (WDM) channels each with CO-OFDM modulation, and Fig. 4(b) shows the zoomed-in optical spectrum for each wavelength channel. We use the bandwidth of the first null to denote the boundary of each wavelength channel [2]. The OFDM bandwidth, B_{OFDM} is thus given by

$$B_{OFDM} = \frac{2}{T_s} + \frac{Nsc-1}{t_s} \tag{9}$$

where t_s is the observation period [Fig. 3(c)]. Assuming a large number of subcarriers used, the bandwidth efficiency of OFDM η is found to be

$$\eta = 2\frac{R}{B_{OFDM}} = 2\alpha, \quad \alpha = \frac{t_s}{T_s} \tag{10}$$

The factor of 2 accounts for two polarizations in the fiber. Using a typical value of 8/9 [1-2], we obtain the optical spectral efficiency factor η of 1.8 Baud/Hz. The optical spectral

#86668 - $15.00 USD Received 20 Aug 2007; revised 1 Nov 2007; accepted 5 Nov 2007; published 9 Jan 2008

efficiency gives 3.6 bit/Hz if QPSK modulation is used for each subcarrier. The spectral efficiency can be further improved by using higher-order QAM modulation [20].

To practically implement CO-OFDM systems, the optical spectral efficiency will be reduced by needing a sufficient guard band between WDM channels taking account of the laser frequency drift about 2 GHz. This guard band can be avoided by using the orthogonality cross the WDM channels, which will be further discussed in the next subsection.

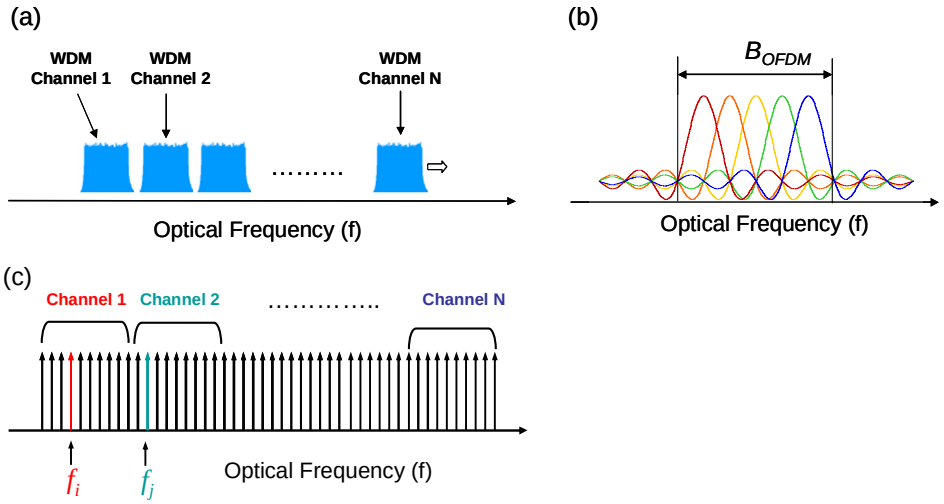

Fig 4. The optical spectrum for (a) *N* wavelength-division-multiplexed CO-OFDM channels, (b) zoomed-in spectrum for one WDM channel, and (c) cross-channel OFDM (XC-OFDM) without guard band.

2.5 Cross-channel OFDM (XC-OFDM): multiplexing without guard band

The laser frequency drift of WDM channels can be resolved by locking all the lasers to the common optical standard such as an optical comb [21]. In so doing, all the subcarriers cross the WDM channels can be orthogonal, i.e., the orthogonality condition of Eqs. (5)-(6) is satisfied for any two subcarriers, even from different WDM channels. As shown in Fig. 4(c), the subcarrier f_i in channel 1 is orthogonal to another subcarrier f_i in different channel (channel 2). We call this form of OFDM cross-channel OFDM (XC-OFDM), namely, the orthogonality applies to the subcarriers from different channels. The term of 'channel' discussed here in a broader sense could be either 'RF' one or 'optical' one, i.e., XC-OFDM can be realized through RF subcarrier multiplexing [5] or wavelength multiplexing shown in Fig. 4(c). An optical or electrical filter with bandwidth slightly larger than the channel bandwidth can be used to select the desired channel. The inter-channel interference is avoided through the orthogonality of XC-OFDM subcarriers. Consequently, no frequency guard band is necessary in such a scheme. However this requires the DFT window synchronization cross WDM channels as we discuss in the section 2.2, which may be difficult to implement. Furthermore, to comply with optical add/drop, a small number of such XC-OFDM channels can be grouped/banded together to allow for guard band between individual group/band, in a similar manner to all-optical OFDM [22].

We would stress the fundamental difference between XC-OFDM proposed here and coherent WDM [23] or all-optical OFDM [22]. First, with XC-OFDM, tight phase stabilization and bit synchronization between WDM channels are not necessary. Second, because OFDM is used in each channel, no optical dispersion compensation is required for XC-OFDM.

#86668 - $15.00 USD Received 20 Aug 2007; revised 1 Nov 2007; accepted 5 Nov 2007; published 9 Jan 2008

3. Channel model for CO-OFDM

The channel model describes the behaviour of communications systems, thus fundamentally determining the performance of the systems. In this section, we will derive a channel model for CO-OFDM systems. Figure 5 shows a complete CO-OFDM system which consists of a CO-OFDM transmitter, an optical link and a CO-OFDM receiver. As thoroughly discussed in [17], the CO-OFDM transmitter comprises an RF OFDM transmitter and RF-to-optical up-converter whereas the CO-OFDM receiver comprises an optical-to-RF down-converter and RF OFDM receiver. Each fibre span consists of chromatic dispersion, multiple stages of high birefringence (HIBI) elements, and polarization dependent loss (PDL) elements. For the sake of simplicity, only one stage of the HIBI and PDL elements are shown. The optical noise is added from the optical amplifiers (OA) at the end of each span.

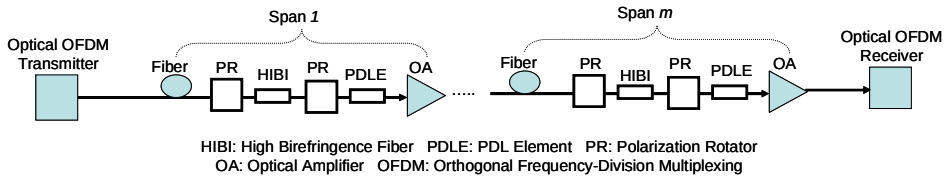

Fig. 5. A complete CO-OFDM system including PMD, PDL and chromatic dispersion effects.

Following the same procedure in [1, 24] , we first arrive at the received OFDM baseband signal in time domain *r(t)* given by

$$r(t) = e^{j\phi(t)} s(t) \otimes h(t) + N(t) \tag{11}$$

$$h(t) = h_t(t) \otimes h_l(t) \otimes h_r(t) \tag{12}$$

where $\phi(t) = \phi_r(t) - \phi_t(t)$, ϕ_t / ϕ_r is the optical OFDM transmitter/receiver phase noise, including optical and RF local oscillator noise, *s(t)* is the transmitted baseband OFDM signal [17]. h_t , h_l and h_r are respectively the impulse response functions for the optical OFDM transmitter, fibre link, and optical OFDM receiver, *h* is overall end-to-end OFDM link impulse response function, *N(t)* is the optical noise added from the OAs throughout the optical fibre link, and '$\otimes$'stands for convolution. The fiber nonlinearity is not considered in this section.

Assuming a perfect DFT window and frequency synchronization, the received signal is sampled and DFT is performed to recover the received OFDM information symbol, which is given by

$$C'_{ki} = I_{i0} \cdot h_{ki} \cdot C_{ki} + \varepsilon_{ki} + n_{ki} \tag{13}$$

$$\varepsilon_{ki} = \sum_{m=-Nsc/2, m\neq k}^{Nsc/2-1} C_{mi} h_{mi} I_{i(m-k)} \tag{14}$$

$$I_{im} = \tfrac{1}{N_{sc}} \sum_{n=-Nsc/2}^{Nsc/2-1} e^{j2\pi nm/Nsc} e^{j\phi_{in}} \tag{15}$$

where C'_{ki} and C_{ki} are respectively the received and transmitted information symbol for the *kth* subcarrier in the *ith* OFDM symbol, ε_{ki} is the inter-carrier interference (ICI) noise induced by the phase noise, n_{ki} is the optical noise from OAs, I_{im} is the ICI coupling coefficient between two subcarriers with distance of *m*, *Nsc* is the number of subcarriers. From Eq. (15),

#86668 - $15.00 USD Received 20 Aug 2007; revised 1 Nov 2007; accepted 5 Nov 2007; published 9 Jan 2008

I_{i0} is expressed as

$$I_{i0} = \frac{1}{N_{sc}} \sum_{n=-Nsc/2}^{Nsc/2-1} e^{j\phi_{in}} \cong \frac{1}{N_{sc}} e^{j\phi_{i0}} \sum_{n=-Nsc/2}^{Nsc/2-1} (1 + j\Delta\phi_{in}) \cong e^{j\phi_i} \tag{16}$$

$$\Delta\phi_{in} = \phi_{in} - \phi_{i0}, \quad \phi_i = \frac{1}{N_{sc}} \sum_{n=-Nsc/2}^{Nsc/2-1} \phi_{in} \tag{17}$$

It can be seen that when $\Delta\phi_{in} << 1$, I_{i0} represents the phase evolution for the entire OFDM symbol, and subsequently ϕ_i can be considered as the OFDM symbol phase (OSP), also known as the common phase error (CPE) [24]. h_{ki} is the frequency-domain channel transfer function given by

$$h_{ki} = h_{ki}^t \cdot h_{ki}^l \cdot h_{ki}^r \tag{18}$$

where h_{ki}^t and h_{ki}^r are respectively the frequency responses of the optical OFDM transmitter and receiver including the responses of DAC/ADC, RF post/preamplifier, optical IQ modulator and balanced photo-detectors. h_{ki}^l is the frequency response of the fibre including chromatic dispersion, PMD and PDL effects given by

$$h_{ki}^l = e^{j\Phi_{ki}^D} \prod_{p=1}^{M} \exp\left\{\left(-\frac{1}{2} j \cdot \vec{\beta}_{pi} \cdot f_k + \frac{1}{2}\vec{\alpha}_{pi}\right) \cdot \vec{\sigma}\right\} \tag{19}$$

$$\Phi_{ki}^D = \pi \cdot c \cdot D_t \cdot f_k^2 / f_{LD}^2 \tag{20}$$

where Φ_{ki}^D is the phase shift due to the chromatic dispersion, f_k is the frequency for the *kth* subcarrier, *M* is the number of the PMD/PDL cascading elements in the entire fibre link with each (e.g., *pth)* section represented by its birefringence vector $\vec{\beta}_p$ and PDL vector $\vec{\alpha}_p$ [25], $\vec{\sigma}$ is the Pauli matrix vector, D_t is the total chromatic dispersion assuming quadratic dependence on frequency but in general can be an arbitrary function of the frequency, f_{LD} is the centre frequency of the transmit/receive laser.

For a large number of subcarriers, ε_{ki} in Eq. (13) can be approximated as the Gaussian noise [26]. Furthermore, the signal processing in this paper is performed on blocks of large number of OFDM symbols, e.g., 100 OFDM symbols per block. The optical channel varies relatively slowly (<10 kHz) and subsequently the channel transfer function within several blocks of OFDM symbols can be considered constant. For the sake of simplicity, the subscript '*i*' for channel transfer function *h* will be dropped, in order to show it is invariant within each OFDM block. Using small phase noise assumption [Eqs. (16, 17)], Eq. (13) becomes

$$C'_{ki} = e^{i\phi_i} h_k C_{ki} + \zeta_{ki} \tag{21}$$

where $\zeta_{ki} = \varepsilon_{ki} + n_{ki}$.

Equations (13) and (21) represent the channel model for CO-OFDM. They can be treated as coherent optical multiple-input multiple-output OFDM (CO-MIMO-OFDM) models [6]. They serve as the starting point for the CO-OFDM signal processing. From the channel models, it follows that to recover OFDM information symbol successfully, the knowledge of channel transfer function h_k and phase ϕ_i is required. The process of determining h_k and ϕ_i are called channel estimation [2,27] and phase estimation (or subcarrier recovery) [2,28],

#86668 - $15.00 USD Received 20 Aug 2007; revised 1 Nov 2007; accepted 5 Nov 2007; published 9 Jan 2008

respectively. We note that the concept of the coherent optical MIMO for the single-carrier system has been introduced and discussed in [29].

4. Optical transmitter design for CO-OFDM

As we have discussed in the section 2.3, the primary design goal for CO-OFDM is to construct a linear transformation system. Consequently, investigation of the nonlinearity of CO-OFDM transmitter is of vital importance. The MZM characteristic has been extensively investigated in [30]. The nonlinearity of MZM on the system performance in the direct-detected systems has been thoroughly studied in [31-32]. It is shown that for the conventional direct-detected system the optimal bias point is at quadrature and a large signal will add nonlinearity impairment to the system. In this section we will focus our attention to the nonlinearity from the OFDM RTO up-converter. We first present the architecture choices for a generic CO-OFDM system. We then formulate the two-tone nonlinearity representation for the RTO up-converter that performs the linear transformation from electrical drive voltage to the optical field.

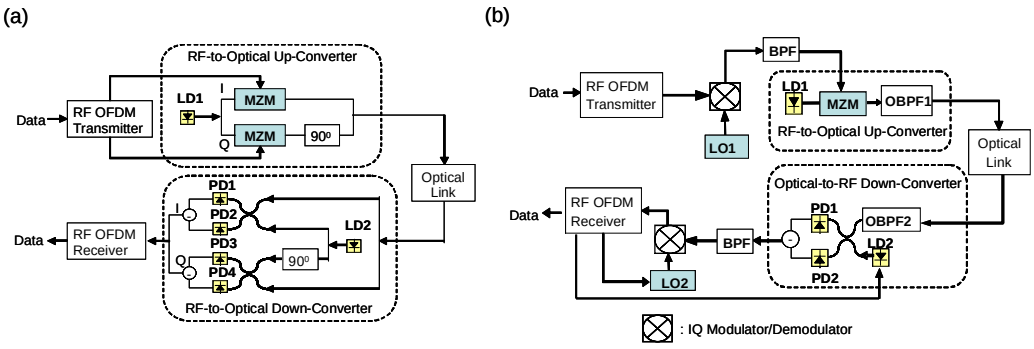

Fig. 6. A CO-OFDM system in (a) direct up/down conversion architecture, and (b) intermediate frequency (IF) architecture.

4.1 Up/down conversion design options for CO-OFDM systems

Figures 6(a) and 6(b) show respectively a CO-OFDM system which uses direct up/down conversion architecture and intermediate frequency (IF) architecture. In the direct up-conversion architecture [Fig. 6(a)], the optical transmitter uses an optical I/Q modulator which comprises two MZMs to up convert the real/imaginary parts of the *s(t)* [Eq. (1)], from the RF domain to the optical domain, i.e., each MZM is respectively driven by the real or imaginary part of the *s(t)*. In the direct down-conversion architecture, the OFDM optical receiver uses two pairs of balanced receivers and an optical 90^0 hybrid to perform optical I/Q detection. The RF OFDM receiver performs OFDM base-band processing to recover the data. The advantages for such a direct-conversion architecture are (i) elimination of a need for image rejection filter in both transmitter and receiver, and (ii) significant reduction of the required electrical bandwidth for both transmitter and receiver. In the intermediate frequency (IF) up-conversion architecture, the OFDM base-band signal is first up-converted to an intermediate frequency f_{LO1} in electrical domain, and the OFDM IF signal is further up-converted to optical domain with one MZM. In the IF down-conversion system, the optical OFDM signal is first down-converted to an intermediate frequency f_{LO2} and the electrical I/Q detection is performed.

Since the transmitter can be of either direct or IF up-conversion architecture, and the receiver can be of either direct or IF down-conversion architecture, there are four design

#86668 - $15.00 USD Received 20 Aug 2007; revised 1 Nov 2007; accepted 5 Nov 2007; published 9 Jan 2008

choices for a CO-OFDM system (only two are shown Fig. 6). Furthermore, at the receive end, direct down-conversion is synonymous with homodyne detection, and IF down-conversion is synonymous with heterodyne detection. However, the terms of direct-conversion and IF transmitter/receiver are already widely-accepted OFDM terminologies, and subsequently are adopted in this paper to encompass the architectures at both transmit and receive ends.

4.2 Two-tone intermodulation analysis

Two-tone analysis is commonly used to characterize RF component and system nonlinearity. In this section, we will use similar two-tone intermodulation analysis to study the MZM nonlinearity upon the RF-to-optical conversion for a CO-OFDM transmitter. The result obtained here should apply to coherent analog multi-carrier systems. For the direct up/down conversion architecture [Fig. 6(a)], two complex subcarrier tones at $v_1 = v \cdot e^{j\omega_1 t}$ and $v_2 = v \cdot e^{j\omega_2 t}$ are applied to the input of the optical I/Q modulator. For the sake of simplicity, we only show the nonlinearity performance analysis for direct up/down conversion architecture. The optical signal at the output of the optical IQ modulator is

$$E(t) = A \cdot \cos\left(\frac{\pi}{2} \cdot \frac{V_I + V_{DC}}{V_\pi}\right) \cdot \exp\left(j\omega_{LD1} t + j\phi_{LD1}\right) + A \cdot \cos\left(\frac{\pi}{2} \cdot \frac{V_Q + V_{DC}}{V_\pi}\right) \exp\left(j\omega_{LD1} t + \pi/2 + j\phi_{LD1}\right) \tag{22}$$

where A is a proportionality constant. All the proportionality constants will be omitted in the remainder of the paper. V_I and V_Q are real and imaginary part of the complex RF drive signal to each MZM, expressed as $V_I = v \cdot (\cos\omega_1 t + \cos\omega_2 t)$, $V_Q = v \cdot (\sin\omega_1 t + \sin\omega_2 t)$, V_{DC} is the DC bias voltage of the modulator, V_π is the half-wave switching voltage, ω_{LD1}/ϕ_{LD1} is the frequency/phase for the transmitter laser. After simple rearrangement, the signal at the output of the optical IQ modulator becomes

$$E(t) = \exp\left(j\omega_{LD1} t + j\phi_{LD1}\right) \cdot E^B(t) \tag{23}$$

$$E^B(t) = \cos\left[\frac{M}{2}(\cos\omega_1 t + \cos\omega_2 t) + \frac{\phi}{2}\right] + j\cos\left[\frac{M}{2}(\sin\omega_1 t + \sin\omega_2 t) + \frac{\phi}{2}\right] \tag{24}$$

where $M = v\pi/V_\pi$ is defined as the modulation index, $\phi = V_{DC}\pi/V_\pi$ is a static phase shift (bias point), and $E^B(t)$ is the equivalent base-band (or frequency down-converted) version of the optical field *E(t)*. The so-defined modulation index *M* equals to the optical modulation index of the optical signal if the optical modulator is biased at quadrature in a direct-detected system. The modulation index *M* defined here is used to characterize the amplitude of the drive voltage, and subsequently it is not limited to the upper bound of 1 as the conventional optical modulation index. We will perform the analysis on $E^B(t)$ for the sake of simplicity, as it is a simple frequency translation of the optical field *E(t)*. The derived nonlinearity expression for $E^B(t)$ will apply to the optical field *E(t)*.

Expanding the cosine term in (24) using Bessel functions, the fundamental output component with frequency $\omega_{1,2}$ can be expressed as

$$E^B_{\omega_{1,2}}(t) = 2 \cdot \sin(\phi/2) \cdot J_0(M/2) \cdot J_1(M/2) \cdot e^{j\omega_{1,2} t} \tag{25}$$

The second-order intermodulation output with frequency $\omega_{1,2} - \omega_{2,1}$ can be expressed as

#86668 - $15.00 USD Received 20 Aug 2007; revised 1 Nov 2007; accepted 5 Nov 2007; published 9 Jan 2008

$$E^{B}_{\omega_{1,2}-\omega_{2,1}}(t) = 2\cdot\cos(\phi/2)\cdot J_1^2(M/2)\cdot e^{j(\omega_{1,2}-\omega_{2,1})t} \tag{26}$$

The third-order intermodulation output with frequency $2\omega_{1,2}-\omega_{2,1}$ will be

$$E^{B}_{2\omega_{1,2}-\omega_{2,1}}(t) = 2\cdot\sin(\phi/2)\cdot J_1(M/2)\cdot J_2(M/2)\cdot e^{j(2\omega_{1,2}-\omega_{2,1})t} \tag{27}$$

We employ the standard nth-order intercept point (IPn) to characterize the modulator nonlinearity [31]. In particular, IP2 (IP3) is the point where the linear extension of the second-order (third-order) intermodulation output power intersects the linear extension of the fundamental output power. The intercept points are given in terms of fundamental output power. IP2 and IP3 are calculated from (25)-(27), and can be expressed as

$$\mathrm{IP2} = 2\cdot\sin^4(\phi/2)/\cos^2(\phi/2) \tag{28a}$$

$$\mathrm{IP3} = 4\cdot\sin^2(\phi/2) \tag{28b}$$

The corresponding intercept points referenced at the input of the optical I/Q modulator are given by the modulation index expressed as

$$M_{IP2} = 2\cdot\tan(\phi/2) \tag{29a}$$

$$M_{IP3} = 4\sqrt{2} \tag{29b}$$

It can be shown that (28b) and (29b) are also valid for the intermediate frequency (IF) architecture, and the second-order nonlinearity is avoided for the intermediate frequency (IF) architecture.

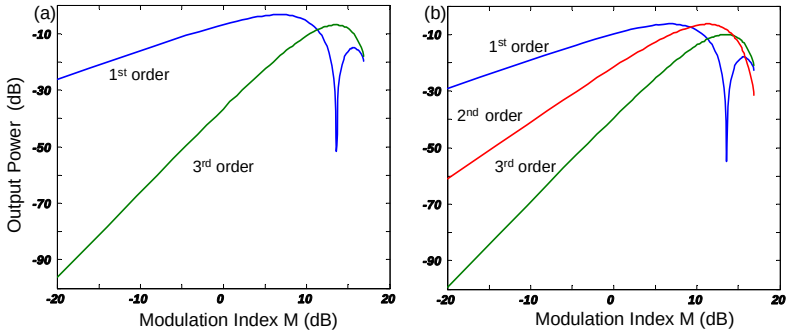

Fig. 7. The first-, second-, and third-order output powers as a function of modulation index *M(dB)=20logM* at the bias points of (a) π, and (b) π/2.

Equation (28b) shows that when modulator is biased at the zero output (ϕ=π), the IP3 has the maximum value, or least non-linearity, which means the optimum bias point should be π. Figures 7(a) and 7(b) show the characteristics of the first-, second-, and third-order intermodulation as a function of the modulation index *M* for a bias point of π and quadrature respectively. It can be seen that at the bias point of π, the fundamental output is maximized while the second-order intermodulation product is eliminated in comparison with the quadrature bias point. In the CO-OFDM systems, any pair of the subcarriers will generate second- and third-order intermodulation products. The system penalty due to the optical I/Q modulator nonlinearity under various bias conditions is thoroughly discussed in [17].

#86668 - $15.00 USD Received 20 Aug 2007; revised 1 Nov 2007; accepted 5 Nov 2007; published 9 Jan 2008

4.3 Discussion of the null bias point of MZM for CO-OFDM systems

The quadrature bias point has been widely adopted for both analog and digital direct-detection systems. The null bias point for CO-OFDM up-conversion signifies a fundamental difference between the optical intensity modulation and optical field modulation. For instance, in coherent detection systems, the transformation between the electrical drive voltage and optical field is of the concern, whereas in the conventional direct detection systems, the transformation between the electrical drive voltage and the optical power is of the concern. Figure 8 shows the transfer functions for both the optical intensity and optical field (I/Q component) against the drive voltage. In Fig. 8, we assume zero initial phase offset between the two arms of MZM at zero bias voltage. The transfer function for the direct detection is the optical intensity against the drive voltage, whereas the transfer function for the coherent detection is the *I/Q* component of the optical field against the drive voltage. It is apparent from Fig. 8 that the optimal MZM bias for optical intensity modulation is quadrature whereas the optimal bias for optical field modulation is the null point.

It is worth noting that the conclusion of the optimal modulator bias of π for the RTO up-conversion is fundamental in dependent of the detailed waveform of $V_{I/Q}$, i.e., $V_{I/Q}$ can be any arbitrary waveform, not necessarily limited to that of CO-OFDM. For instance, for direct-detection optical OFDM, it is still optimal to bias the modulator at null point to minimize RTO up-conversion nonlinearity. However, the challenge there is how to reinsert the main optical carrier, which is lost due to the bias at null point. We anticipate a great deal of original research effort taking advantage of this linear transformation between the optical field and electrical drive voltage in coherent or incoherent, digital or analog systems.

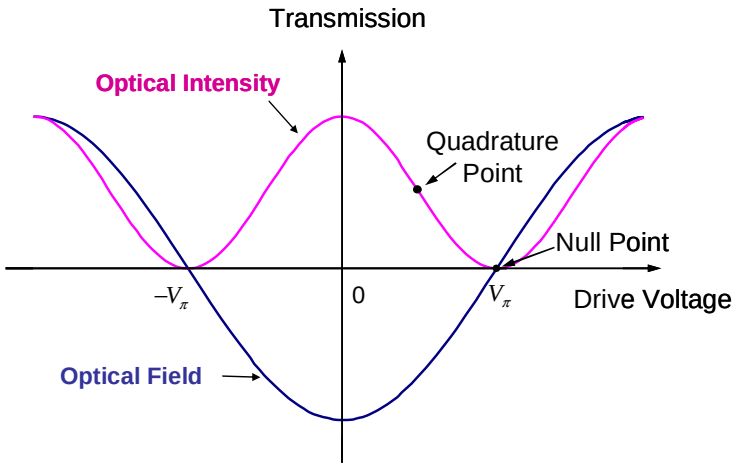

Fig. 8. The transfer functions for the optical intensity and the optical field against the drive voltage.

5. Nonlinearity compensation with receiver digital processing for CO-OFDM

Because of the large peak-to-average-power-ratio (PAPR) inherent for CO-OFDM signals, we expect that the CO-OFDM is sensitive to the fiber nonlinearity. Nevertheless, it has been shown that the system Q of the WDM channels at 10 Gb/s is over 13.0 dB for a transmission up to 4800 km of standard-single-mode-fiber (SSMF) without dispersion compensation [33]. The system Q of the WDM channels can be further improved by using a technique of partial carrier filling (PCF) [33]. With a filling factor of 50 % at 10 Gb/s, the system Q factor is improved from 15.1 dB to 16.8 dB for a transmission up to 3200 km of SSMF without dispersion compensation [33]. However, the major disadvantage of PCF is that the bandwidth efficiency is significantly reduced. The first attempt to mitigate the nonlinear phase noise through receiver digital signal processing has been recently reported for CO-OFDM systems

#86668 - $15.00 USD Received 20 Aug 2007; revised 1 Nov 2007; accepted 5 Nov 2007; published 9 Jan 2008

[6]. However, that work is only limited to a lump nonlinear compensation at the receiver. In this section, we will extend that work by using digital phase conjugation and distributed nonlinearity compensation, which is equivalent of reverse signal propagation proposed for single-carrier coherent detection [34].

5.1 Principle of receiver-based phase noise mitigation: digital phase conjugation (DPC)

Mid-span phase conjugation has been proposed to mitigate the nonlinear phase noise [35-36]. Figure 9 shows a transmission system employing optical phase conjugation, where the two identical fiber spans (fiber span I and fiber span II) are sandwiched with a phase conjugator (PC). It has been shown that by using mid-span phase conjugation, the self phase modulation (SPM) can be perfectly removed, and Gordon-Mollenauer phase noise can be significantly reduced [35-36]. The digital signal processing we propose here is to digitally implement the phase conjugation and propagation of the signal through fiber span II. Because of coherent detection used in CO-OFDM where the optical field is sampled digitally, the phase conjugation can be simply completed by performing a phase conjugation of the sample received signal. We would like to point out that the mid-span phase conjugation interpretation of the signal processing is identical to the reverse propagation scheme proposed for the single-carrier coherent detection systems [34]. We chose to use the mid-span phase conjugation interpretation to stress that both SPM and Gordon-Mollenauer phase noise are reduced by receiver-based digital processing. In a hardware-based phase conjugated system [35-36], the PC needs to be placed at a fixed location, which is undesirable for a dynamic network where an optical connection can be added/dropped at any point of the network. The distinct advantage for the receiver-based DPC is that it can be readily performed in response to any dynamic connection. The disadvantage of such an approach is the added computation complexity.

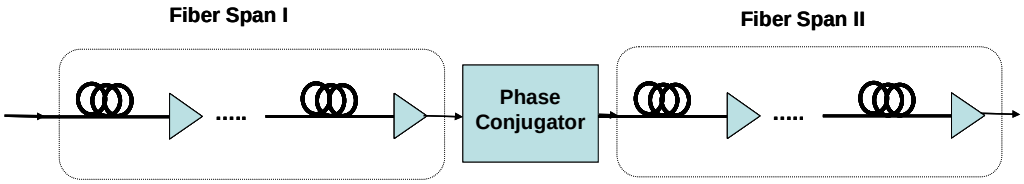

Fig. 9. A transmission system with mid-span phase conjugation

The challenge for DPC scheme is how to digitally propagate the optical field through the 'fiber span II' in Fig. 9. It is known that the fiber propagation is governed by the nonlinear Schrodinger equation [37]. Theoretically, the nonlinear propagation can be performed using split-step Fourier method with a very fine step. However, this would be computation-intensive and impractical to implement in real-time. We thus need to approximate the entire 'fiber span II' as a few limited segments of nonlinearity and chromatic dispersion operations, as shown in Fig. 10. The simplest configuration will be one segment of nonlinearity and chromatic dispersion each. This is in essence the lump nonlinearity compensation, which has been recently demonstrated [6]. Mathematically the digital signal processing on the received signal r(t) is given by [37]

$$r_0(t) = \left(\prod_{i=2}^{m} \exp\left(\hat{N}_i\right) \exp\left(\hat{D}_i\right) \right) \exp\left(\hat{N}_1\right) r^*(t) \tag{30}$$

$$\hat{N}_i A(t) = j\beta \left| A_i(t) \right|^2 \tag{31}$$

$$\hat{D}_i A(t) = \left\{ F^{-1} \exp\left(j\phi_D \right) F \right\} A(t) \tag{32}$$

#86668 - $15.00 USD Received 20 Aug 2007; revised 1 Nov 2007; accepted 5 Nov 2007; published 9 Jan 2008

where $r_0(t)$ is the phase noise mitigated waveform, $\hat{N}_i$ and $\hat{D}_i$ respectively are the nonlinearity operator and chromatic dispersion operator for the *ith* segment [37], *F* is the Fourier transfer function, ϕ_D is the dispersion for the *ith* segment, and *A(t)* is a generic OFDM signal waveform. We stress here that algorithm laid out in Eqs. (30)-(32) is compatible to the FFT algorithm in the CO-OFDM transmitter and receiver. Therefore, the same FFT engine in the chip for CO-OFDM symbol modulation/demodulation can be reused for nonlinearity mitigation.

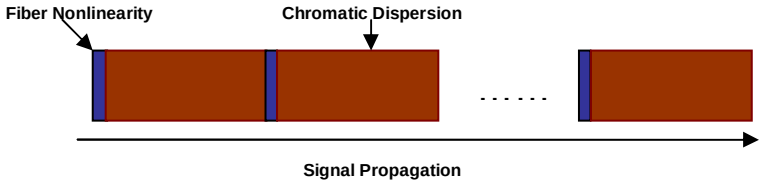

Fig. 10. Abstraction of the split-step Fourier method for signal propagation in the fiber

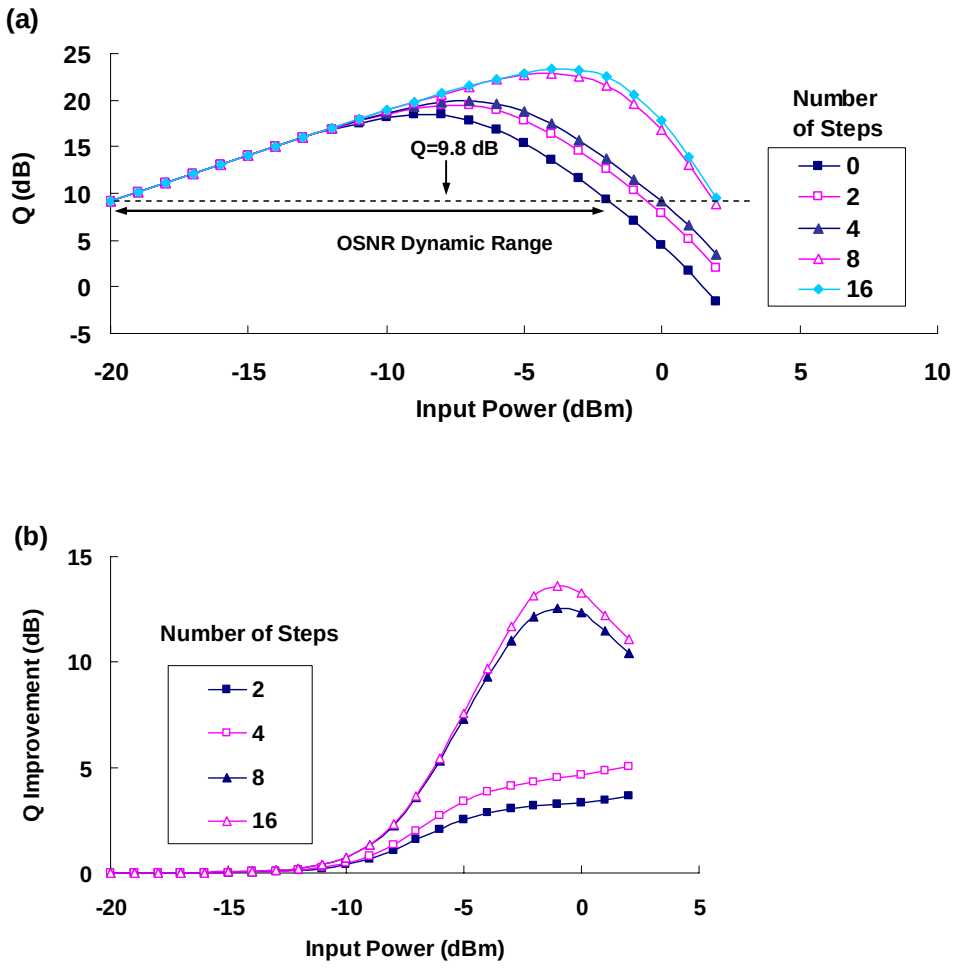

Fig. 11. (a). The Q factor as a function of the launch power with varying number of steps used in split-step Fourier method in nonlinear phase noise mitigation, and (b) the Q factor improvement as a result of nonlinear noise phase noise mitigation.

#86668 - $15.00 USD Received 20 Aug 2007; revised 1 Nov 2007; accepted 5 Nov 2007; published 9 Jan 2008

5.2 Simulation results of receiver-based digital processing for nonlinearity mitigation

A Monte Carlo simulation is conducted to investigate the nonlinear phase noise mitigation for the CO-OFDM system. The OFDM parameters are OFDM symbol period of 25.6 ns, 128 subcarriers, a guard interval equal to one quarter of the observation period, QPSK encoding for each subcarrier. We apply commonly used system parameters for our simulation: 80 km span distance, fiber chromatic dispersion of 16 ps/nm/km, 0.2 dB/km loss, and a nonlinear coefficient of 2.6×10^{-20} m^2/W. The fiber span loss is compensated by an EDFA with a gain of 16 dB and noise figure of 6 dB. The linewidth of the LD1 and LD2 are assumed to be 100 kHz, which is close to the value achieved with commercially available semiconductor lasers [38]. The CO-OFDM system configuration is identical to that in [33] where a direct up/down conversion architecture has been adopted. In this paper, we limit our analysis to single-channel transmission.

We first conduct a transmission simulation for a reach of 1600 km, with the receiver digital processing including digital phase conjugation and split-step Fourier nonlinear propagation. The results are shown in Fig. 11. The number of steps corresponds to the number of partition segments in the split-step Fourier method. It can be seen from Fig. 11(a) that as the number of steps increases, the system Q is improved, and the optimal launched power increases to a higher value. In particular, the optimal launch power without nonlinear mitigation is -9 dBm whereas the optimal launch power increases to -4 dBm if 8 steps are used. Figure 11(b) shows the Q improvement as a function of launch power with varying number of steps. As expected, the dramatic improvement takes place at the high launch powers beyond -5 dBm. Even for a two-step processing, a Q improvement of larger than 3 dB is obtained when the launch power is above -5 dBm. It can be seen that the improvement rolls off at the step of 8, which means that the partitioned fiber length is 200 km, which seems to be sufficient for nonlinear phase mitigation. It is interesting to note that for large number steps (>8), although the Q factor has been improved though launching more power, the Q declines more steeply when the launch power is beyond the optimal value. This is evidenced by the fact that there exists an optimal launch power for the Q improvement for large number of steps, as shown in Fig. 11(b). Furthermore, the optimal Q may not be the best indicator for measuring system margin in CO-OFDM system, as intentional clipping of OFDM signals may generate background error floor. We propose using the OSNR dynamic range to measure the system margin. As shown in Fig. 11(a), the OSNR dynamic range is defined as the launch power dynamic range that both lower end and higher end coincides with a Q value of 9.8 dB, a correctable BER through FEC.

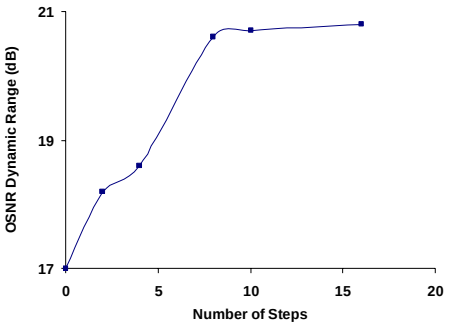

Fig. 12. OSNR dynamic range as a function of number of steps.

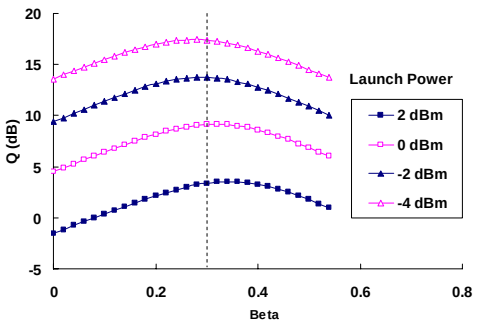

Fig. 13. The Q factor as the function of the nonlinear coefficient β for a step size of 4.

#86668 - $15.00 USD Received 20 Aug 2007; revised 1 Nov 2007; accepted 5 Nov 2007; published 9 Jan 2008

Using the definition of OSNR dynamic range, the performance of nonlinear phase noise mitigation is shown in Fig. 12. It shows that the OSNR dynamic range is improved from 17 dB to 20.6 dB with 8-step nonlinear phase noise mitigation. It is interesting to note that the corresponding optimal Q is improved from 18.5 dB to 22.9 dB, showing 4.4 dB improvement.

The amount of nonlinear mitigation is adjusted by varying β, a phenomenological nonlinear coefficient in Eq. (31). Obviously β is optical link dependent. It can be estimated whenever a new connection is initiated through optimization of the actual BER. It is important that once β is optimized, it should apply to any other arbitrary launch power. We verify this assumption by performing simulation under different launch powers. Figure 13 shows the Q factor as a function of nonlinear coefficient β with the step size of 4. It can be seen that if a value of 0.3 is selected for β, it should work for a wide dynamic range of the launch power. The simulation results for different steps arrive at the same conclusion.

6. Conclusion

In this paper, we have first reviewed the theoretical fundamentals for CO-OFDM. We then present various design choices for CO-OFDM systems as well as the nonlinearity analysis for OFDM RF-to-optical up-converter. We also show the receiver-based digital signal processing to mitigate self-phase modulation (SPM) and Gordon-Mollenauer phase noise.

Acknowledgment

This work was supported by the Australian Research Council (ARC).

#86668 - $15.00 USD Received 20 Aug 2007; revised 1 Nov 2007; accepted 5 Nov 2007; published 9 Jan 2008